Check for updates

An on-site and portable electrochemical sensing platform based on spinel zinc ferrite nanoparticles for the quality control of paracetamol in pharmaceutical samples†

Nguyen Tuan Anh, [ID] ‡*[a] Le Minh Tung,‡*[c] Le Khanh Vinh,[d] Nguyen Van Quy,[e] Ong Van Hoang,[af] Ngo Xuan Dinh [ID] [a] and Anh-Tuan Le [ID] *[ab]

In this study, crystalline spinel zinc ferrite nanoparticles ($ZnFe_2O_4$ NPs) were successfully prepared and proposed as a high-performance electrode material for the construction of an electrochemical sensing platform for the detection of paracetamol (PCM). By modifying a screen-printed carbon electrode (SPE) with $ZnFe_2O_4$ NPs, the electrochemical characteristics of the $ZnFe_2O_4$/SPE and the electrochemical oxidation of PCM were investigated by cyclic voltammetry (CV), electrochemical impedance spectroscopy (EIS), chronoamperometry (CA), and differential pulse voltammetry (DPV) methods. The calculated electrochemical kinetic parameters from these techniques including electrochemically active surface area (ECSA), peak-to-peak separation (ΔE_p), charge transfer resistance (R_{ct}), standard heterogeneous electron-transfer rate constants (k^0), electron transfer coefficient (α), catalytic rate constant (k_{cat}), adsorption capacity (Γ), and diffusion coefficient (D) proved that the as-synthesized $ZnFe_2O_4$ NPs have rapid electron/mass transfer characteristics, intrinsic electrocatalytic activity, and facilitate the adsorption–diffusion of PCM molecules towards the modified electrode surface. As expected, the $ZnFe_2O_4$/SPE offered excellent analytical performance towards sensing of PCM with a detection limit of 0.29 μM, a wide linear range of 0.5–400 μM, and high electrochemical sensitivity of 1.1 μA μM^{-1} cm^{-2}. Moreover, the proposed $ZnFe_2O_4$-based electrochemical nanosensor also exhibited good repeatability, high anti-interference ability, and practical feasibility toward PCM sensing in a pharmaceutical tablet. Based on these observations, the designed electrochemical platform not only provides a high-performance nanosensor for the rapid and highly efficient detection of PCM but also opens a new avenue for routine quality control analysis of pharmaceutical formulations.

1. Introduction

Paracetamol (PCM) also known as acetaminophen or *N*-acetyl-*p*-aminophenol is one of the most widely available and commonly used antipyretic and analgesic drugs.[1,2] PCM has been used for more than a century as an effective and safe treatment for relieving pain (headache, backache, muscular aches, arthritis, and post-operative pains) and reducing fever.[3,4] Generally, PCM is relatively free of side effects at the normal therapeutic doses, but hypersensitivity, overdoses, or regular use of PCM can cause amassing of toxic metabolites which leads to hepatic toxicity, and liver and kidney damage.[5–7] Owing to its low cost and easy accessibility, the growing production of PCM drug results in increasing amounts of poor-quality pharmaceuticals in global public health, leading to potential risks to human health. Therefore, monitoring the PCM doses in a given pharmaceutical formulation is crucial for quality control, stability testing, identification, and clinical studies before being licensed for circulation in the commercial market.

To date, many analytical methods have been employed for the determination of PCM content in pharmaceutical formulations including spectrophotometry,[8] high-performance liquid chromatography,[9] titrimetry,[10] spectrofluorimetry,[11] UV-Vis spectroscopy,[8]

[a]*Phenikaa University Nano Institute (PHENA), PHENIKAA University, Hanoi 12116, Vietnam. E-mail: anh.nguyentuan1@phenikaa-uni.edu.vn; tuan.leanh@phenikaa-uni.edu.vn*

[b]*Faculty of Materials Science and Engineering, PHENIKAA University, Hanoi 12116, Vietnam*

[c]*Department of Physics, Tien Giang University, My Tho City, Tien Giang Province, Vietnam. E-mail: leminhtung@tgu.edu.vn*

[d]*National Institute of Applied Mechanics and Informatics, Vietnam Academy of Science and Technology (VAST), Ho Chi Minh 70000, Vietnam*

[e]*International Training Institute for Materials Science (ITIMS), Hanoi University of Science and Technology (HUST), 01 Dai Co Viet Road, Hanoi 10000, Vietnam*

[f]*University of Transport Technology, Trieu Khuc, Thanh Xuan District, Hanoi, Viet Nam*

† Electronic supplementary information (ESI) available. See DOI: https://doi.org/10.1039/d3na00749a

‡ N. T. Anh and L. M. Tung contributed equally to this work.

gas chromatography,[12] and capillary electrophoresis.[13] Nevertheless, these quantification techniques are unsuitable for performing routine, rapid, and on-site analysis due to the requirements for sophisticated expensive instruments, time-consuming sampling, skilled operators, and centralized laboratories. For this reason, it is imperative to develop rapid, sensitive, cost-effective, and efficient detection methods for quantitative determination of PCM. Since PCM is an electroactive compound and the mechanism of electrochemical oxidation/reduction has been systematically investigated,[1,14,15] electrochemical sensors have attracted widespread attention and great potential in the pharmaceutical quality control of PCM. Owing to the inherent advantages including rapid analysis time, cost-effectiveness, facile miniaturization, on-site detection, high sensitivity and selectivity,[16–18] the electrochemical sensor can be used as a promising sensing platform for the determination of PCM. To date, numerous electrochemical sensors have been developed for the electrochemical detection of PCM. Rohini M. Hanabaratti et al.[19] reported an economical and efficient glassy carbon electrode (GCE) modified with zinc oxide NPs for quantitative determination of PCM. Jayant I. Gowda et al.[20] prepared a GCE modified with multiwalled carbon nanotube-cetyltrimethyl ammonium bromide for PCM oxidation detection in medical, pharmaceutical and biotechnological real samples. Recently, Edgar Nagles et al.[21] developed a new method based on a carbon paste electrode (CPE) and La_2O_3 to detect and quantify PCM in tablets, powder and syrup with PCM.

Nowadays, with the rapid development of nanoscience and nanotechnology, the usage of nanomaterials as signal amplification components has attracted tremendous attention in the construction of a high-performance electrochemical sensing platform for the ultra-sensitive detection of targeted analytes.[16,22,23] When nanomaterials are introduced into the electrode surface, the electrochemical kinetic parameters can be comprehensively improved, leading to considerable enhancement in the overall analytical performance.[24,25] Recently, spinel oxide-based nanostructures have become quite popular modifiers due to their advantages such as low cost, chemical stability, rich redox properties, superior catalytic activity, and fast electron transfer kinetics.[26,27] Particularly, many research and review articles have investigated and summarized the use of various spinel nanostructures such as spinel ferrite (AFe_2O_4), spinel cobaltite (MCo_2O_4), and zinc oxide spinel (ZnB_2O_4) as electrochemical sensors.[27–29] In recent work, our group developed a series of electrochemical sensors based on AFe_2O_4 (A = Zn, Co, Mn, Ni, Cu), BCo_2O_4 (B = Zn, Cu), and $ZnFe_2O_4/ZnO$ hetero-nanostructures for the highly sensitive detection of various types of analytes including chloramphenicol, furazolidone, carbaryl, and clenbuterol.[30–34] Therefore, the electrochemical sensing platform and spinel oxide nanostructures are expected to provide a promising combination for quickly and accurately analysing as well as quantifying pharmaceutical tablets.

In the present work, a spinel zinc ferrite ($ZnFe_2O_4$) nanomaterial was successfully prepared by a facile hydrothermal method and applied to the electrochemical determination of PCM. The developed $ZnFe_2O_4$-modified electrode possesses rapid electron/mass transfer properties, fabulous electrocatalytic activity, and enhanced adsorption/diffusion capacity

compared to the bare screen-printed electrode (SPE). With the rapid growth of the screen-printing technique, SPEs with the advantages of cost-effectiveness, small size, and easy integration have proven to be a powerful tool to overcome the limitations of conventional three-electrode systems (CPE, GCE) such as requiring repeated recalibration, complicated pre-treatment, and being inappropriate for on-site analysis. As a result, the $ZnFe_2O_4$/SPE-based electrochemical sensor has splendid electroanalytical performance towards the electro-oxidation of PCM with high electrochemical sensitivity, low limit of detection, wide linear dynamic range, good repeatability, and excellent anti-interference ability. Furthermore, the developed electrochemical sensing platform based on the $ZnFe_2O_4$-modified SPE was successfully applied for quantifying the amounts of PCM drug in commercially available pharmaceutical formulations with satisfactory recovery value. Our proposed rapid-sensing platform and portable electrochemical device would open new avenues for the precise, sensitive, efficient, and on-site detection of PCM in pharmaceutical and urine samples.

2. Experimental procedures

2.1. Chemicals and reagents

Zinc nitrate hexahydrate $Zn(NO_3)_2 \cdot 6H_2O$, iron(III) nitrate nonahydrate $Fe(NO_3)_3 \cdot 9H_2O$, ethylene glycol $(CH_2OH)_2$, and sodium hydroxide (NaOH) were supplied by Xilong Scientific Co., Ltd. Potassium chloride (KCl), potassium dihydrogen phosphate (KH_2PO_4), sodium chloride (NaCl), and dibasic sodium phosphate (Na_2HPO_4) were manufactured by Merck KGaA, Germany. A pure sample of PCM powder obtained from the National Institute of Drug Quality Control of Vietnam was used as standard. All the reagents used were of analytical grade and all of the aqueous solutions were prepared using deionized (DI) water.

2.2. Synthesis of $ZnFe_2O_4$ NPs

$ZnFe_2O_4$ NPs were synthesized using a hydrothermal method, combined with subsequently annealing treatment based on the previously published literature.[31] In brief, appropriate quantities of $Zn(NO_3)_2 \cdot 6H_2O$ and $Fe(NO_3)_3 \cdot 9H_2O$ with the molar ratio of 1 : 2 were added into 80 mL of a DI water/ethylene glycol mixture (1 : 1 volumetric ratio). Afterward, 2 M aqueous NaOH solution was added dropwise to the above homogeneous mixture to form a dark red precipitate. After stirring for 10 minutes, the obtained solution was sealed in a Teflon-lined stainless-steel autoclave and reacted at 180 °C for 12 h. After being cooled naturally to room temperature, the obtained product was harvested by centrifugation and washed with ethanol and DI water before drying at 60 °C for 24 h. Finally, the $ZnFe_2O_4$ NPs were produced by calcining the powder at 500 °C for 5 h in air.

2.3. Fabrication of the $ZnFe_2O_4$-modified electrode

The $ZnFe_2O_4$-modified SPE electrode was prepared via a facile drop-casting method. First, 1 mg of the as-prepared $ZnFe_2O_4$ NPs was dispersed in 1 mL of DI water by ultrasonic treatment for 3 h to form a homogeneous suspension. Then, an 8 μL aliquot of the $ZnFe_2O_4$ suspension was dripped onto the

working surface of the bare SPE and dried at room temperature. Finally, the $ZnFe_2O_4$/SPE was preserved at 4 °C in a refrigerator for subsequent electrochemical experiments.

2.4. Electrochemical measurements

All electrochemical measurements including cyclic voltammetry (CV), electrochemical impedance spectroscopy (EIS), chronoamperometry (CA), and differential pulse voltammetry (DPV) techniques were performed using a Palmsens 4 electrochemical workstation (PS Trace, Palmsens, The Netherlands).

The characterization of the bare SPE and $ZnFe_2O_4$/SPE was carried out by CV and EIS techniques. CV was carried out in 0.1 M KCl solution containing 5 mM $K_3[Fe(CN)_6]$/$K_4[Fe(CN)_6]$ within the potential range of 0.6 to −0.2 V. The EIS technique was applied using an AC voltage amplitude of 10 mV in 0.1 M KCl containing 5 mM $[Fe(CN)_6]^{3-/4-}$ solution in the frequency range of 0.01 Hz to 100 kHz.

The electrochemical behavior of PCM on the bare SPE and $ZnFe_2O_4$/SPE was investigated using CV, CA, and DPV measurements. Phosphate buffer electrolyte solution (0.1 M PBS) was adopted as the electrolyte for electrochemical experiments. CV measurement was conducted in the potential range between 0.5 and 1.2 V. CA measurements were done at an applied potential of 0.35 V. For the determination of linear range, the limit of detection, and electrochemical sensitivity for PCM at the $ZnFe_2O_4$-modified electrode, the DPV technique was performed in the potential range from 0.6 to 1.2 V at a scan rate of 6 mV s^{-1} in 0.1 M PBS containing different concentrations of PCM.

2.5. Real samples preparation

Commercial pharmaceutical tablets containing 500 mg of PCM were purchased from a local drug store in Hanoi, Vietnam. Initially, ten pieces of 10 tablets were accurately weighed and finely pulverized, and then 50 mg of the homogenized powder was dissolved in 50 mL 0.1 M PBS (pH 5.0). The obtained solution was stirred for 3 h at room temperature and filtered through Whatman filter paper. The clear supernatant liquid was subsequently collected and diluted with 0.1 M PBS (pH 5.0) to obtain the concentration of PCM in the working range. In order to perform PCM assay in human urine samples, the standard addition method was used. 5 mL of PCM free-human urine sample was obtained from a healthy volunteer (male: 27 years, 72 kg, 173 cm). 5 mL of urine sample was added to 5 mL of a 0.1 M PBS solution (pH 5.0), and then mixed with a vortex mixer. Finally, the known different amounts (50, 200, and 400 μM) of PCM standards were added. The recovery tests were carried out using the DPV technique and the ultimate concentration of PCM in the tablet and human urine samples was calculated from three repeated DPV measurements and the regression equation of the calibration curve.

3. Results and discussion

3.1. Physical characterization

The crystal structure of the $ZnFe_2O_4$ sample was characterized by powder X-ray diffraction (XRD) measurement using an EQUINOX 5000 diffractometer with Cu Kα radiation (λ = 0.154056 nm). The XRD, Raman, and field emission scanning electron microscopy (FE-SEM) results are described in Fig. 1. The XRD pattern of the $ZnFe_2O_4$ nanomaterials matches well with the single phase cubic spinel structure (JCPDS no. 22-1012), confirming the highly crystalline and single-phase formation of the $ZnFe_2O_4$. The three well-defined characteristic Raman peaks of $ZnFe_2O_4$ at 350, 495, and 655 cm^{-1} can be assigned to F_{2g} (2), F_{2g} (3), and A_{1g} modes, respectively. The morphology of the samples was observed by FE-SEM, which revealed that the as-prepared $ZnFe_2O_4$ are spherical, well dispersed with particle size in the range of 9–21 nm and an average particle size of 14.2 nm. Full information about the synthetic $ZnFe_2O_4$ NPs is reported in our previous paper.[31]

3.2. Electrochemical characteristics of the unmodified and $ZnFe_2O_4$-modified electrodes

The electrochemical activities of the unmodified and $ZnFe_2O_4$-modified SPE electrodes were investigated *via* CV and EIS techniques by using $[Fe(CN)_6]^{3-}$/$[Fe(CN)_6]^{4-}$ as the model redox couple. Fig. 2a depicts the CV curves of the bare SPE and $ZnFe_2O_4$/SPE in 5 mM $[Fe(CN)_6]^{3-/4-}$ containing 0.1 M KCl at a scan rate of 70 mV s^{-1}. There was a pair of well-defined and reversible redox peaks that corresponded to the one-electron transfer process of Fe^{2+} reversibly into Fe^{3+}. Comparing the oxidation and reduction peak current responses at the bare SPE and $ZnFe_2O_4$/SPE, it can be concluded that the modification of the SPE working electrode with $ZnFe_2O_4$ NPs can significantly increase the electron transfer rate. Namely, the calculated results show that the oxidation and reduction peak currents of the $ZnFe_2O_4$/SPE (234.7 and 258.0 μA) were 1.42 and 1.64 times higher than those of the bare SPE (165.0 and 157.0 μA), respectively (Fig. 2b).

The improved charge transfer kinetics was further confirmed by the variation in specific surface area, namely, the electrochemically active surface area (ECSA). The ECSA values of the unmodified and $ZnFe_2O_4$-modified electrodes were estimated based on the CV technique at different scan rates in 0.1 M KCl containing 5 mM $[Fe(CN)_6]^{3-/4-}$ (Fig. S1a and c†) and the Randles–Sevcik equation:[35]

$$\Delta I_p = 2.69 \times 10^5 n^{3/2} D^{1/2} A C \nu^{1/2} \tag{1}$$

where I_p (μA) refers to the oxidation/reduction peak current, n is the number of electrons transferred ($n = 1$), D represents the diffusion coefficient of $[Fe(CN)_6]^{3-/4-}$ ($D = 6.5 \times 10^{-6}$ cm^2 s^{-1}), A (cm^2) is the ECSA, C is the $[Fe(CN)_6]^{3-/4-}$ solution concentration ($C = 5$ mM), and ν (V s^{-1}) is the scan rate. As can be seen in Fig. S1b and d,† the redox current intensity shows a linear correlation with the square root of scan rate at all electrodes, demonstrating a diffusion-controlled electrode process.[31,32] Its linear regression equation was expressed as:

For SPE:

$$\Delta I_{pa} \text{ (μA)} = 468.99 \nu^{1/2} \text{ (V s}^{-1}) + 44.80/R^2 = 0.985$$

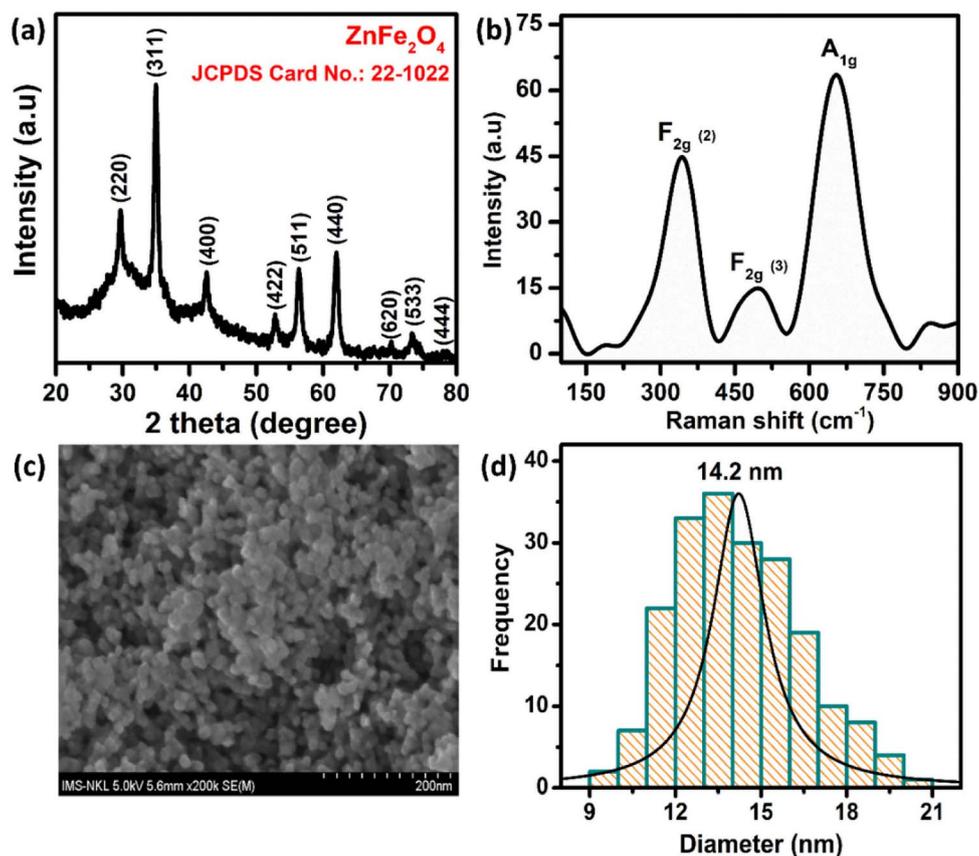$$\Delta I_{pc} \text{ (μA)} = -447.12 \nu^{1/2} \text{ (V s}^{-1}) - 42.34/R^2 = 0.986$$

Fig. 1 (a) XRD pattern, (b) Raman spectrum, (c) the FE-SEM image, and (d) the histogram of particle size distribution of $ZnFe_2O_4$ NPs.

For $ZnFe_2O_4$/SPE:

$$\Delta I_{pa} (\mu A) = 772.32\nu^{1/2} (V\ s^{-1}) + 34.87/R^2 = 0.993$$

$$\Delta I_{pc} (\mu A) = -905.18\nu^{1/2} (V\ s^{-1}) - 28.20/R^2 = 0.980$$

From the obtained slope of the plot of $I_p \sim \nu^{1/2}$, the ECSA values of the bare SPE and $ZnFe_2O_4$/SPE were calculated to be about 0.130 and 0.264 cm², respectively. The ECSA value of the

$ZnFe_2O_4$-modified electrode was 2.03 times higher with respect to the bare SPE, suggesting that the $ZnFe_2O_4$ NPs not only provide more electrochemically active sites in the redox reaction but also accelerate the electron and mass transport at the electrode/electrolyte interface, and thus substantially increase the overall electrochemical performance.

EIS measurements were also carried out to study the charge-transfer kinetics at the electrode/electrolyte interface and measure the electron transfer resistance (R_{ct}) as well as the heterogeneous electron-transfer rate constant (k^0) values.
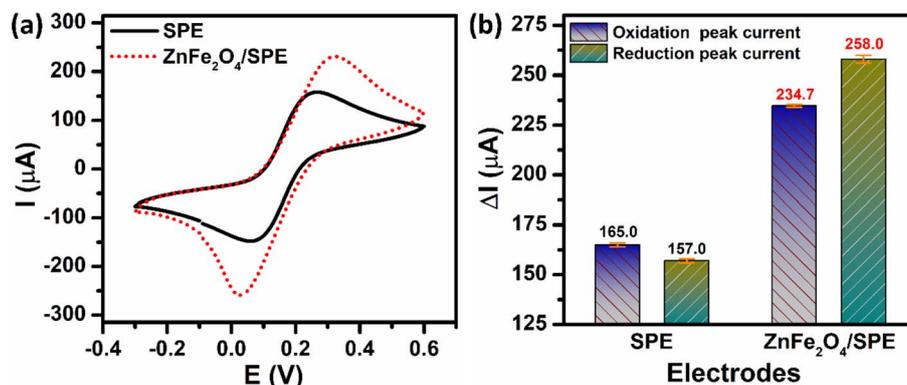

Fig. 2 (a) CV curves and (b) the bar diagram of the oxidation/reduction peak currents of the $ZnFe_2O_4$/SPE in 5 mM $[Fe(CN)_6]^{3-/4-}$ solution containing 0.1 M KCl at a scan rate of 70 mV s⁻¹.
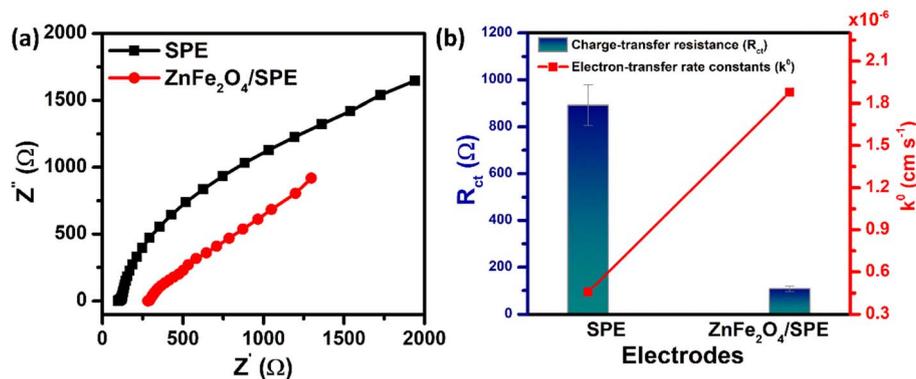
Fig. 3 (a) EIS plots in 5 mM $[Fe(CN)_6]^{3-/4-}$ solution containing 0.1 M KCl for the unmodified and $ZnFe_2O_4$-modified SPE; (b) the bar chart diagram of the charge-transfer resistance (R_{ct}) and the heterogeneous electron-transfer rate constant (k^0) value of the bare SPE and $ZnFe_2O_4/SPE$.

Fig. 3a displays the EIS spectra of the unmodified and $ZnFe_2O_4$-modified electrodes in the supporting electrolyte of 0.1 M KCl containing 5 mM $[Fe(CN)_6]^{3-/4-}$. By using the Randles circuit as a fitting model, the R_{ct} values of the bare SPE and $ZnFe_2O_4/SPE$ were measured to be 891.8 and 105.7 Ω, respectively (Fig. S2†). Furthermore, the heterogeneous electron-transfer rate constant (k^0) values of the bare SPE and $ZnFe_2O_4/SPE$ can be calculated from the obtained ECSA and R_{ct} values using the equation:[18]

$$k^0 = \frac{RT}{n^2 F^2 A C R_{ct}} \quad (2)$$

where R represents gas constant (R = 8.314 J mol^{-1} K^{-1}), T stands for thermodynamic temperature (T = 298.15 K), and F is the Faraday constant (F = 96 485.33 C mol^{-1}). According to that, the calculated k^0 values determined for the bare SPE and $ZnFe_2O_4/SPE$ were 4.58×10^{-7} and 1.88×10^{-6} cm s^{-1}, respectively (Fig. 3b). As expected, the lower R_{ct} value and the higher k^0 value of the $ZnFe_2O_4/SPE$ as compared to the bare SPE indicate that the $ZnFe_2O_4$-modified electrode possesses excellent electronic conductivity and rapid electron/mass transport ability between the electrode surface and analyte molecules. On the basis of the CV and EIS measurements as well as the calculated characteristic parameters, thanks to unique features including large specific surface area, abundant active sites, high electrical conductivity, and continuous electron transport at the

electrode/electrolyte interface for excellent electrochemical behaviors, the as-synthesized $ZnFe_2O_4$ nanomaterials enable it to be an ideal sensing platform in constructing high-performance electrochemical sensors.

3.3. Electrochemical behaviors of PCM at the unmodified and $ZnFe_2O_4$-modified electrodes

The electrochemical performance of the unmodified and $ZnFe_2O_4$-modified electrodes towards the determination of PCM was investigated by the CV technique in 0.1 M PBS (pH 5.0) containing 50 μM PCM at a scan rate of 70 mV s^{-1}. As shown in Fig. 4a, both the bare SPE and $ZnFe_2O_4/SPE$ exhibited two couples of well-defined anodic/cathodic peaks of PCM molecules. However, the $ZnFe_2O_4$-modified electrode had a considerable effect on the electrochemical activity (Fig. 4b). Namely, for the bare SPE, the cathodic and anodic peak potentials (E_{pa} and E_{pc}) of PCM were observed at 375.1 and 185.3 mV with the oxidation and reduction peak currents (I_{pa} and I_{pc}) being calculated to be about 3.08 and 2.24 μA, respectively. Impressively, for the $ZnFe_2O_4/SPE$, the I_{pa} and I_{pc} values of the PCM redox reaction were 1.61 and 1.75-fold higher than those of the bare SPE (4.96 and 3.91 μA) with the E_{pa} and E_{pc} values being located at 290.2 and 190.3 mV, respectively. The values of peak-to-peak potential separation ($\Delta E_p = |E_{pa} - E_{pc}|$) are one of the
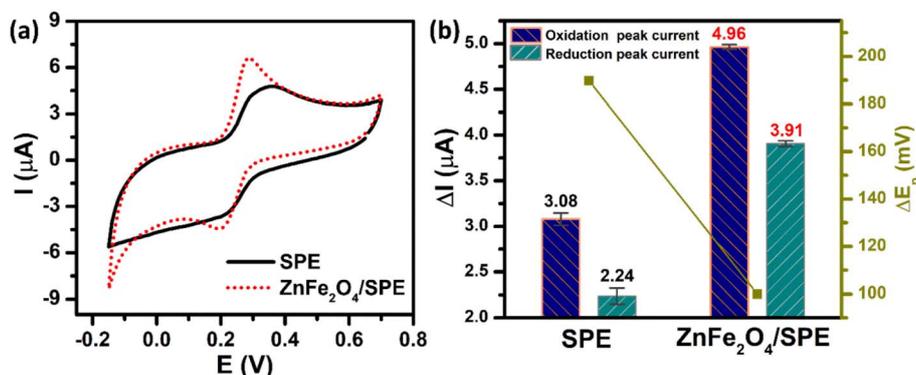

Fig. 4 (a) CV curves and (b) the bar diagram of redox peak currents of 50 μM PCM in 0.1 M PBS (pH 5.0). The scan rate of CV is 70 mV s^{-1}.
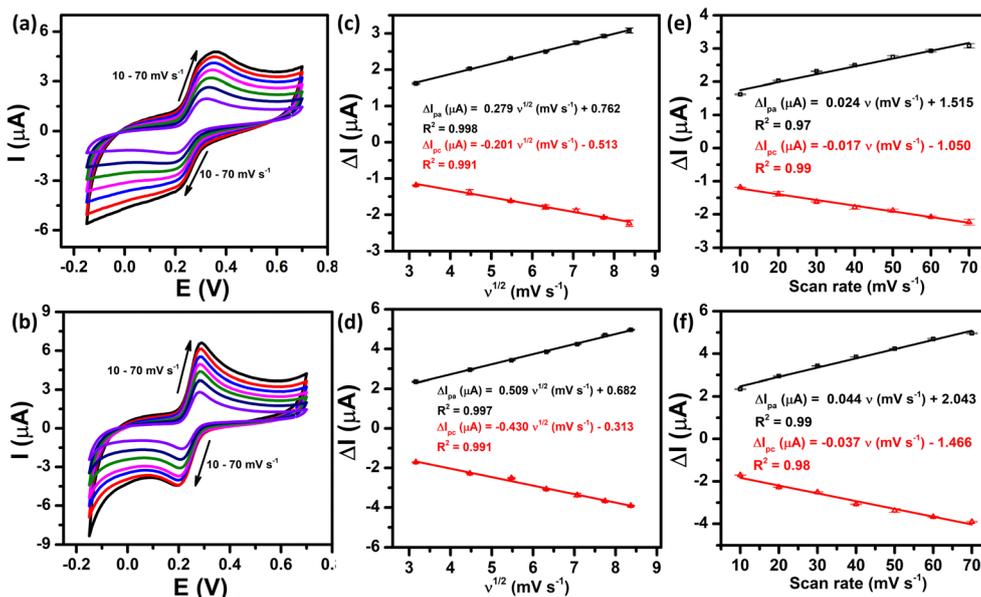
Fig. 5 CV curves recorded at the bare SPE and ZnFe$_2$O$_4$/SPE in 0.1 M PBS (pH 5.0) containing 50 μM PCM at different scan rates (a) and (b), plots of peak current *vs.* square root of scan rate (c) and (d), and plots of peak current *vs.* scan rate (e) and (f), respectively.

most important electron transfer kinetic parameters that need to be calculated. According to that, the unmodified SPE has a large ΔE_p value of 189.8 mV, illustrating the sluggish electron transferability. The ZnFe$_2$O$_4$-modified electrode displays a decreased in the ΔE_p value, which was measured to be about 99.9 mV, indicative of the fast electron-transfer kinetics relative to the bare SPE.

The electron transfer coefficient (α) is another kinetic parameter utilized to characterize the electronic properties of an electrode material, and can be calculated by using Laviron's equation:[36]

$$E_{pc} = E^{0'} - RT\frac{\ln \nu}{\alpha nF} \quad (3)$$

$$E_{pa} = E^{0'} + RT\frac{\ln \nu}{(1-\alpha)nF} \quad (4)$$

where $E^{0'}$ is the formal peak potential, which was calculated from the midpoint of cathodic and anodic peak potentials and R, T, n, and F have their usual meanings. As expected, the α value of the ZnFe$_2$O$_4$/SPE (0.99) was ~1.55 times higher than that of the bare SPE (0.64), which demonstrates that introducing ZnFe$_2$O$_4$ nanomaterials into the electrochemical sensing platform can effectively accelerate the rate of electron transfer on the working electrode.

The electrochemical kinetics of the PCM redox reactions were further clarified by exploring the influence of scan rate on the anodic and cathodic peak currents. Fig. 5a and b demonstrate the CV curves of the bare SPE and ZnFe$_2$O$_4$/SPE at different scan rates from 10 to 70 mV s^{-1} in 0.1 M PBS (pH 5.0) containing 50 μM PCM. As can be observed at both electrodes, the redox peak currents increased linearly with increasing the square root of scan rate, confirming the PCM redox reaction at

the bare SPE and that ZnFe$_2$O$_4$/SPE is a diffusion-controlled process[37,38] (Fig. 5c and d).

For SPE:

$$\Delta I_{pa} \text{ (μA)} = 0.279\nu^{1/2} \text{ (mV s}^{-1}) + 0.762/R^2 = 0.998$$

$$\Delta I_{pc} \text{ (μA)} = -0.201\nu^{1/2} \text{ (mV s}^{-1}) - 0.513/R^2 = 0.991$$

For ZnFe$_2$O$_4$/SPE:

$$\Delta I_{pa} \text{ (μA)} = 0.509\nu^{1/2} \text{ (mV s}^{-1}) + 0.682/R^2 = 0.997$$

$$\Delta I_{pc} \text{ (μA)} = -0.430\nu^{1/2} \text{ (mV s}^{-1}) - 0.313/R^2 = 0.991$$

Furthermore, there is a good linear relationship between the redox peak currents *vs.* scan rate, indicating that both the oxidized and reduced forms are confined to the surface, confirming the surface controlled pseudocapacitive behavior[39] (Fig. 5e and f).

For SPE:

$$\Delta I_{pa} \text{ (μA)} = 0.024\nu \text{ (mV s}^{-1}) + 1.515/R^2 = 0.97$$

$$\Delta I_{pc} \text{ (μA)} = -0.017\nu \text{ (mV s}^{-1}) - 1.050/R^2 = 0.99$$

For ZnFe$_2$O$_4$/SPE:

$$\Delta I_{pa} \text{ (μA)} = 0.044\nu \text{ (mV s}^{-1}) + 2.043/R^2 = 0.99$$

$$\Delta I_{pc} \text{ (μA)} = -0.037\nu \text{ (mV s}^{-1}) - 1.466/R^2 = 0.98$$

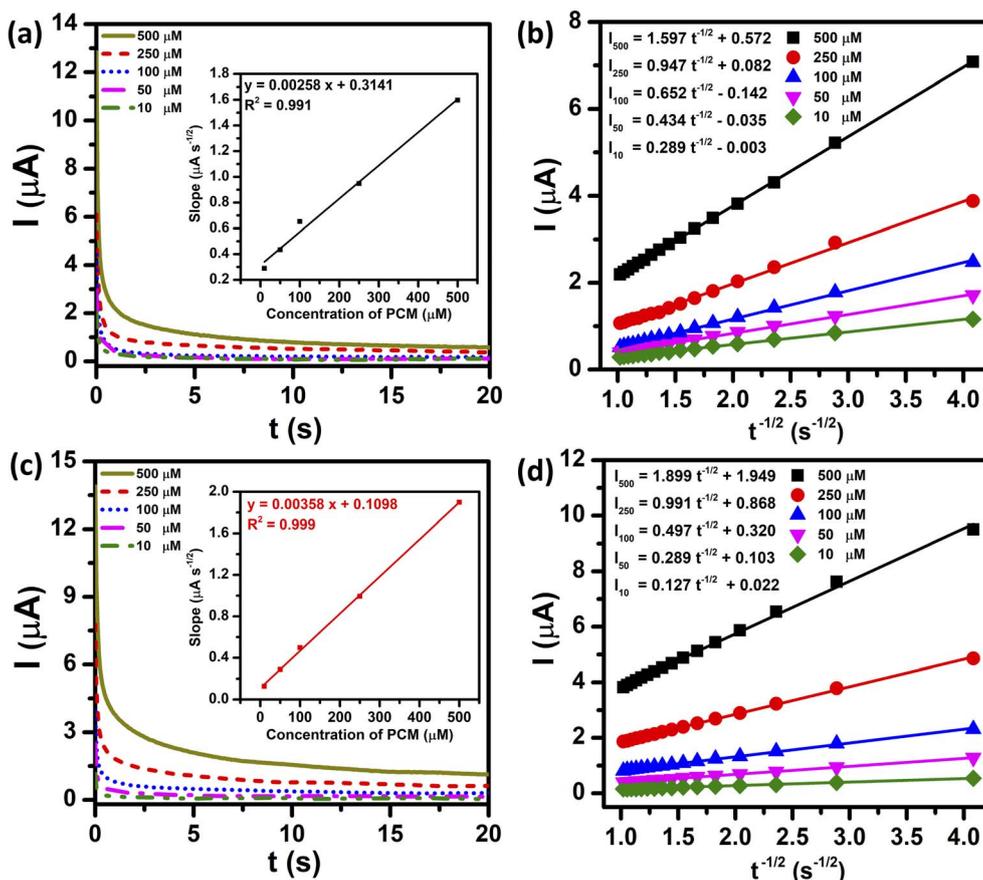**Fig. 6** Chronoamperograms at the bare SPE and ZnFe$_2$O$_4$/SPE for different concentrations of PCM from 10 to 500 μM in 0.1 M PBS (pH 5.0) (a) and (c) and plot of I vs. $t^{-1/2}$ obtained from chronoamperograms (b) and (d). Inset shows the plot of slopes of the resulting straight lines against PCM concentration.

To sum up, the oxidation/reduction peak currents of PCM showed a good linearity with both the scan rate and the square root of the scan rate. Therefore, it can be concluded that all the electrode reactions have been identified as a combination of diffusion-controlled and surface-controlled pseudocapacitive redox systems. These results are consistent with the redox behavior of PCM in the previous studies.[25,40] More interestingly, from the obtained slope values of the plot of $I_p \sim \nu$, the adsorption capacity (Γ) was measured using the following equation:[41]

$$\Delta I_p = \frac{n^2 F^2 A \nu \Gamma}{4RT} \tag{5}$$

According to that, the adsorption capacities of PCM at the bare SPE and ZnFe$_2$O$_4$/SPE were approximately 3.31×10^{-8} and 4.37×10^{-8} mol cm^{-2}, respectively.

Two parameters reflecting the enhancement in the electrocatalytic activity for the redox reaction of PCM at both unmodified and ZnFe$_2$O$_4$-modified electrodes, namely diffusion

Table 1 The characteristic parameters of electrochemical redox reactions of the [Fe(CN)$_6$]$^{3-/4-}$ and PCM using the bare SPE and ZnFe$_2$O$_4$/SPE

Characteristic parameters	Electrodes	
	SPE	ZnFe$_2$O$_4$/SPE
The electrochemically active surface area, ECSA (cm^2)	0.130	0.264
The charge transfer resistance, R_{ct} (Ω)	891.8	107.5
The heterogeneous electron-transfer rate constants, k^0 (cm s^{-1})	4.58×10^{-7}	1.88×10^{-6}
The peak-to-peak separation, ΔE_p (mV)	189.9	99.9
The electron transfer coefficient, α	0.64	0.99
The adsorption capacity, Γ (mol cm^{-2})	3.31×10^{-8}	4.37×10^{-8}
The catalytic rate constant, k_{cat} (M^{-1} s^{-1})	4.67×10^6	6.51×10^6
The diffusion coefficient, D (cm^2 s^{-1})	7.17×10^{-8}	1.01×10^{-7}

coefficient (D) and catalytic rate constant (k_{cat}), were evaluated by the CA technique. Fig. 6a and c show the CA results of diverse concentrations of PCM (10, 50, 100, 250, and 500 μM) in 0.1 M PBS (pH 5.0), with the potential being set at 350 mV. As shown in Fig. 6b and d, the anodic current response shows linear dependency upon the negative square root of time ($I \sim v^{-1/2}$) at different PCM concentrations, indicating that the electrocatalytic reaction of PCM is predominantly controlled by diffusion. Consequently, the D values of PCM molecules at the bare SPE and ZnFe$_2$O$_4$/SPE can be determined using the Cottrell equation:[42]

$$I = nFAD^{1/2}C_b\pi^{-1/2}t^{-1/2} \tag{6}$$

where I is the chronoamperometric response (A), C_b the bulk concentration of PCM (mol cm^{-3}), and t is the elapsed time (s). From the slopes of the I against $v^{-1/2}$ plots, these resultant straight line slopes were plotted $vs.$ PCM concentration and are shown in the inset of Fig. 6a and c, which can be expressed as follows:

For SPE: slope $= 0.00258C_{PCM} + 0.3141/R^2 = 0.991$

For ZnFe$_2$O$_4$/SPE: slope $= 0.00358C_{PCM} + 0.1098/R^2 = 0.999$

Consequently, using the Cottrell equation and resultant slopes, the diffusion coefficients of PCM of the bare SPE and ZnFe$_2$O$_4$/SPE were determined to be 7.17×10^{-8} and 1.01×10^{-7} cm s^{-1}, respectively.

The CA measurement was also used for the investigation of the electrocatalytic activity of the ZnFe$_2$O$_4$-modified electrode toward the electro-oxidation of PCM. Fig. S3a and c† illustrate the CA curves obtained for the electrochemical oxidation of PCM on the bare SPE and ZnFe$_2$O$_4$/SPE in 0.1 M PBS (pH 5.0) in the absence and presence of 500 μM PCM. The catalytic rate constant (k_{cat}) for the oxidation of PCM is calculated based on the time–current curve and the Galus equation:[42]

$$I_C/I_L = \pi^{1/2}(k_{cat}C_b t)^{1/2} \tag{7}$$

where I_C and I_L are the catalytic current and diffusion-limited current in the presence and absence of PCM, respectively. As shown in Fig. S3b and d,† the I_C/I_L value was linearly dependent on the square root of time ($t^{1/2}$) with the regression equations being expressed as follows:

For SPE: $I_C/I_L = -38.29t^{1/2} + 79.37/R^2 = 0.986$

For ZnFe$_2$O$_4$/SPE: $I_C/I_L = -45.23t^{1/2} + 124.70/R^2 = 0.986$

As a result, from the slopes of the I_C/I_L against $t^{1/2}$ plot, the k_{cat} value is calculated to be 4.67×10^6 M^{-1} s^{-1} for the bare SPE and 6.51×10^6 M^{-1} s^{-1} for the ZnFe$_2$O$_4$/SPE.

The characteristic parameters of electrochemical redox reactions of the $[Fe(CN)_6]^{3-/4-}$ couple and PCM molecules at the bare SPE and ZnFe$_2$O$_4$/SPE such as ECSA, R_{ct}, k^0, ΔE_p, α, Γ, and k_{cat} are summarized in Table 1. Taken together, the most striking result to emerge from these data is that the employment of ZnFe$_2$O$_4$ nanomaterials as electrode surface modifiers has direct and significant positive effects on the overall electrochemical performance. The unique features of spinel oxide nanostructures not only endow the ZnFe$_2$O$_4$ with high electroactive surface areas and plentiful accessible active sites, which led to a substantial increase in electrical conductivity and conductive channels for ion/electron transfer but also improve the quantity of adsorption of analyte molecules on the electrode active surface, thereby boosting its overall electrochemical performance. Thus, the ZnFe$_2$O$_4$-modified electrode could be used as a promising sensing platform for high-performance electrochemical sensor construction for ultrasensitive detection of PCM.

3.4. Optimization of electrochemical parameters

In order to achieve high electrochemical sensitivity, wide linear range, and low limit of detection for the determination of PCM, the DPV technique was used. Prior to the optimization stage, the DPV oxidation peak current and DPV reduction peak current of PCM need to be compared due to the electrochemical reaction
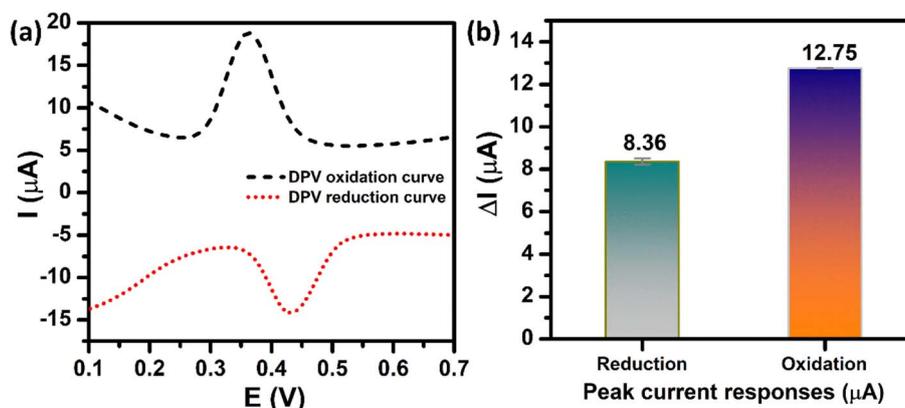

Fig. 7 (a) DPV oxidation/reduction curves and (b) the bar diagram of the oxidation/reduction peak currents of the ZnFe$_2$O$_4$/SPE in 0.1 M PBS (pH 5.0) containing 250 μM PCM.

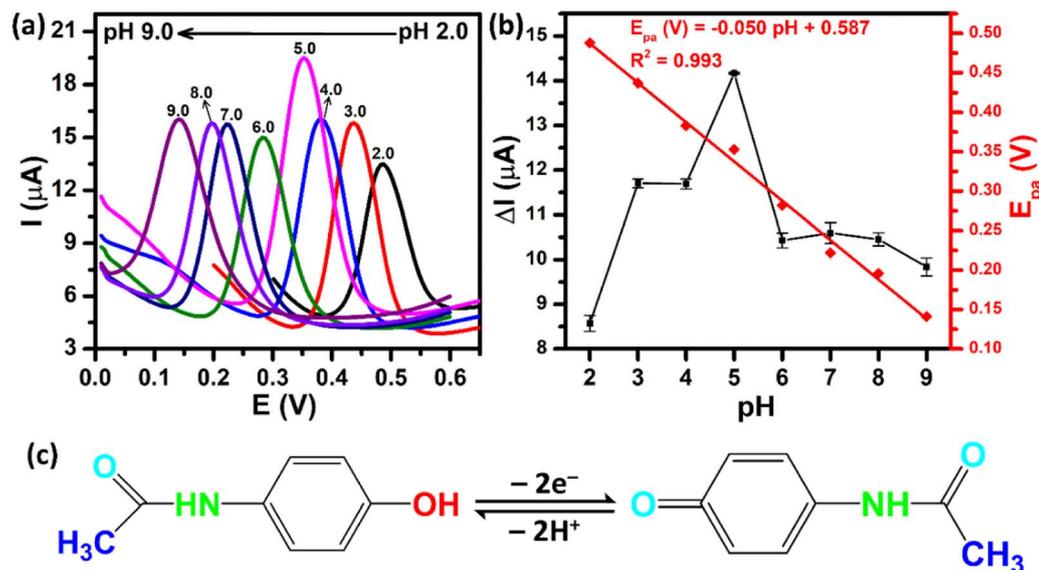**Fig. 8** (a) DPV curves of 250 μM PCM at ZnFe$_2$O$_4$/SPE with different pH values from 2.0 to 9.0; (b) calibration plots of ΔI_{pa} and E_{pa} against pH values; (c) the electrochemical oxidation mechanism of PCM.

of PCM occurring at the ZnFe$_2$O$_4$-modified electrode being a reversible process. Fig. 7a depicts the DPV behaviors of electrochemical oxidation and reduction of PCM at the ZnFe$_2$O$_4$-modified electrode. The two peaks at 0.36 V and 0.43 V can be attributed to the electro-oxidation and electro-reduction of PCM molecules, respectively. As shown in Fig. 7b, the oxidation peak current of PCM (12.75 μA) was ~1.53-fold larger than that of the reduction peak current of PCM (8.36 μA). Therefore, the electrochemical oxidation process using the DPV technique was chosen to achieve the highest analytical performance toward the detection of PCM.

Effect of pH. The supporting electrolyte pH is one of the major factors in improving the sensing performance. Fig. 8a shows the DPV curves of the ZnFe$_2$O$_4$/SPE in the presence of 250 μM PCM over the pH range from 2.0 to 9.0. As can be observed, the oxidation peak potentials of PCM shifted to a negative value

with the increase of pH, illustrating that electrons and protons are involved in the electrochemical oxidation process of PCM. From the obtained DPV curves, the plots of the peak currents and peak potentials as a function of the pH values were drawn, as shown in Fig. 8b. The oxidation peak currents of PCM gradually increased when the pH value was changed from 2.0 to 5.0, and then decreased gradually when the pH value was over 5.0. Therefore, pH 5.0 (PBS 0.1 M) was chosen as an appropriate electrolyte to obtain the best sensitivity for further electrochemical experiments. Furthermore, the oxidation peak potentials of PCM were directly proportional to the pH values with the linear fitting equation being expressed as E_{pa} (V) = −0.05 pH + 0.587 with R^2 = 0.993. The slope of −0.05 V pH^{-1} was close to the Nernst theoretical value (−0.059 V pH^{-1}), suggesting that the oxidation process of PCM occurred under an equal number of protons and electrons (Fig. 8c). The obtained
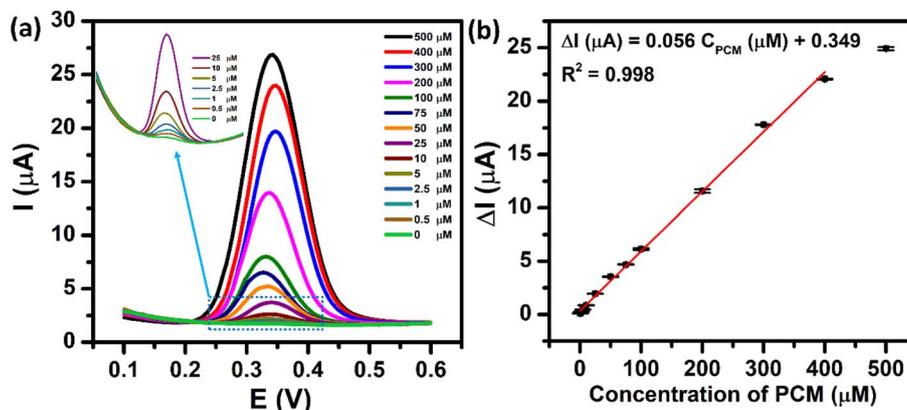

Fig. 9 (a) DPV curves of 0–500 μM PCM in 0.1 M PBS (pH 5.0) at the ZnFe$_2$O$_4$/SPE and (b) the calibration plots of oxidation peak current responses *vs.* various concentrations of PCM with error bars.

results further confirmed that the electrochemical oxidation of PCM occurring on the surface of the $ZnFe_2O_4$-modified electrode was reversible, similar to the previous reports.[20,43]

Effect of the modified amount and the accumulation time. The modified amount and the accumulation time are crucial factors in enhancing the analytical performance. The influence of the accumulation time upon the electrochemical signal has been examined in the range from 30 to 180 s (Fig. S4a†). As shown in Fig. S4b,† with the increasing accumulation time from 30 to 150 s, the oxidation peak current of PCM showed a distinct increasing trend. When the accumulation time was further extended, the oxidation peak current of PCM got saturated, implying the maximum adsorption capacity of the PCM on the surface of the $ZnFe_2O_4$-modified electrode. Thus, 150 s was selected as the optimal accumulation time for subsequent experiments.

The influence of the $ZnFe_2O_4$ modifier (1 mg mL^{-1}) on the electrooxidation of PCM was investigated by varying the modified amount in the range from 2 to 10 μL (Fig. S4c and d†). It can be observed that the oxidation peak current increased gradually as the modified amount was increased from 2 to 8 μL. With further increasing the modified amount, the formation of a thick $ZnFe_2O_4$ modifier on the electrode surface may reduce the electrochemically active site area and electrical conductivity of the modified electrode, leading to a decrease in the peak current. Consequently, an optimal modified amount of 8 μL was selected in the following electrochemical experiments.

3.5. Electrochemical determination of PCM at the $ZnFe_2O_4$-modified SPE electrodes

The electrochemical sensing performance of the proposed $ZnFe_2O_4$-modified electrode towards the PCM detection was evaluated by the DPV technique under the optimized conditions. Fig. 9a shows the DPV curves of different concentrations of PCM ranging from 0.5 to 500 μM. As expected, the oxidation peak current of PCM increased with the rising concentrations in the range of 0.5–400 μM. The resulting calibration plots exhibited a good linear relationship between the oxidation peak currents and concentrations of PCM, which can be expressed as $\Delta I_{pa} (\mu A) = 0.056\, C_{PCM} (\mu M) + 0.349$ with $R^2 = 0.998$. The limit of detection (LOD) of the proposed electrochemical sensor was

determined to be 0.29 μM, using the standard formula: LOD $= 3S_D/S$ (where S_D is the standard deviation of 10 blank samples and S is the slope value). Furthermore, from the obtained slope value, the electrochemical sensitivity of the $ZnFe_2O_4$-based electrochemical sensor was calculated to be 1.1 μA μM^{-1} cm^{-2}. The analytical parameters of the $ZnFe_2O_4$-based electrochemical sensor for the detection of PCM are compared with those reported in the recent literature (Tables S1 and S2†). These outcomes indicate that the proposed $ZnFe_2O_4$-based electrochemical sensor exhibited an excellent performance towards the electro-oxidation of PCM with high electrochemical sensitivity, comparatively low limit of detection, and wide linear response ranges.

3.6. Repeatability, anti-interference ability, and real sample analysis

The repeatability of the proposed electrochemical sensor was evaluated by conducting 10 consecutive DPV measurements in 0.1 M PBS (pH 5.0) containing 250 μM PCM (Fig. S5†). As shown in Fig. S5a,† the oxidation responses of PCM showed a negligible change after 10 repeated operations using the $ZnFe_2O_4$-modified electrode under the sample condition. The relative standard deviation (RSD) value was calculated to be 0.76%, indicative of excellent repeatability (Fig. S5b†).

The anti-interference ability was also investigated by adding 20-fold concentration of possible interfering ions (K^+, Na^+, Cu^{2+}, Zn^{2+}, and Fe^{3+}), organic compounds (4-nitrophenol, ascorbic acid, and glucose), and antibiotics (azithromycin, erythromycin, ofloxacin, furazolidone, and chloramphenicol) to a 250 μM PCM (Fig. S6†). The obtained and calculated results manifest that these potential interferences did not cause significant changes in the electro-oxidation of PCM, indicating a good anti-interfering ability during the PCM electro-oxidation of the proposed $ZnFe_2O_4$-based electrochemical sensor for the detection of PCM.

The feasibility of the proposed $ZnFe_2O_4$-modified electrode for the practical application was studied with the electrochemical measurement of PCM in the commercial pharmaceutical product and human urine samples. The ultimate concentration of PCM in tablet and urine samples was calculated from three repeated DPV measurements and the

Table 2 Electrochemical detection of PCM in the commercial pharmaceutical tablet and human urine samples using the $ZnFe_2O_4$-modified electrode

Sample	Labeled values (μM)	Found values[a] (μM)	Recovery (%)	RSD (%)
Pharmaceutical	400	411.1	102.8	0.9
	200	192.9	96.3	1.1
	100	100.9	97.7	0.7
	50	50.6	101.2	2.9
	25	26.6	106.2	0.6
Urine	400	390.5	97.6	0.2
	200	199.3	99.7	2.2
	50	55.5	110.9	0.7

[a] Each sample was assayed in triplicate ($n = 3$).

regression equation of the calibration curve. The results are shown in Table 2. The proposed electrochemical sensor exhibited an excellent recovery range from 96.3 to 110.9%, with the RSD values below 2.9%, demonstrating that the electrochemical sensing platform based on the $ZnFe_2O_4$ NPs can be used as a reliable and feasible method for quantitative analysis of PCM in pharmaceutical formulations and urine samples.

4. Conclusions

In summary, the highly crystalline and single-phase spinel $ZnFe_2O_4$ NPs were successfully synthesized by a facile hydrothermal method and utilized as an electrode material for the construction of an electrochemical sensor for the detection of PCM. A series of electrochemical techniques (CV, EIS, CA, and DPV) along with the calculated electrochemical kinetic parameters (ECSA, R_{ct}, k^0, ΔE_p, α, Γ, k_{cat}, and D) showed that the modification of the SPE working surface with $ZnFe_2O_4$ NPs comprehensively improved the analytical performance toward the PCM detection as compared to the bare SPE. Benefiting from the plenty of active sites and large specific surface area for electrochemical reaction, the $ZnFe_2O_4$-modified electrode shows superior electron transfer capability, good electrocatalytic activity, and large adsorption/diffusion capacity for the electro-oxidation of PCM. As a result, the $ZnFe_2O_4$/SPE shows excellent sensing performance in electrochemical detection of PCM with very low LOD, ultra-wide working range, high electrochemical sensitivity, good anti-interference ability, and satisfactory repeatability. Moreover, the practical applicability of the proposed electrochemical sensor was established with admirable recovery results in the determination of PCM in pharmaceutical tablets and human urine samples.

Author contributions

N. T. Anh: methodology, validation, investigation, writing-original draft; M. T. Le: funding acquisition, conceptualization, methodology, formal analysis; L. K. Vinh: validation, investigation; N. V. Quy: validation, formal analysis; O. V. Hoang: validation, investigation; N. X. Dinh: conceptualization, methodology, supervision, formal analysis, writing-review & editing; L. A. Tuan: conceptualization, methodology, supervision, project administration, writing-review & editing.

Conflicts of interest

The authors declare that they have no known competing financial interests or personal relationships that could have appeared to influence the work reported in this paper.

Acknowledgements

References

1 M. E. Bosch, A. J. R. Sánchez, F. S. Rojas and C. B. Ojeda, *J. Pharm. Biomed. Anal.*, 2006, **42**, 291–321.

2 R. N. Goyal, V. K. Gupta, M. Oyama and N. Bachheti, *Electrochem. Commun.*, 2005, 7, 803–807.

3 M. Boopathi, M.-S. Won and Y.-B. Shim, *Anal. Chim. Acta*, 2004, **512**, 191–197.

4 R. T. Kachoosangi, G. G. Wildgoose and R. G. Compton, *Anal. Chim. Acta*, 2008, **618**, 54–60.

5 K. V Blake, D. Bailey, G. M. Zientek and L. Hendeles, *Clin. Pharm.*, 1988, 7, 391–397.

6 K. J. Heard, *N. Engl. J. Med.*, 2008, **359**, 285–292.

7 Y. Fan, J.-H. Liu, H.-T. Lu and Q. Zhang, *Colloids Surf., B*, 2011, **85**, 289–292.

8 A. R. Khaskheli, A. Shah, M. I. Bhanger, A. Niaz and S. Mahesar, *Spectrochim. Acta, Part A*, 2007, **68**, 747–751.

9 A. W. Abu-Qare and M. B. Abou-Donia, *J. Pharm. Biomed. Anal.*, 2001, **26**, 939–947.

10 K. G. Kumar and R. Letha, *J. Pharm. Biomed. Anal.*, 1997, **15**, 1725–1728.

11 J. Vilchez, R. Blanc, R. Avidad and A. Navalón, *J. Pharm. Biomed. Anal.*, 1995, **13**, 1119–1125.

12 A. Trettin, A. A. Zoerner, A. Böhmer, F.-M. Gutzki, D. O. Stichtenoth, J. Jordan and D. Tsikas, *J. Chromatogr. B*, 2011, **879**, 2274–2280.

13 A. Kunkel, S. Günter and H. Wätzig, *Electrophoresis*, 1997, **18**, 1882–1889.

14 A. Kutluay and M. Aslanoglu, *Anal. Chim. Acta*, 2014, **839**, 59–66.

15 K. Asadpour-Zeynali and R. Amini, *Electroanalysis*, 2017, **29**, 635–642.

16 N. T. Anh, N. X. Dinh, T. N. Pham, L. K. Vinh, L. M. Tung and A.-T. Le, *RSC Adv.*, 2021, **11**, 30544–30559.

17 E. Bakker and M. Telting-Diaz, *Anal. Chem.*, 2002, **74**, 2781–2800.

18 N. T. Anh, N. X. Dinh, N. N. Huyen, P. T. L. Huong, V. N. Phan, P. D. Thang, H. Van Tuan, T. Van Tan and A.-T. Le, *J. Electrochem. Soc.*, 2023, **170**, 17510.

19 R. M. Hanabaratti, S. M. Tuwar, S. T. Nandibewoor and J. I. Gowda, *Chem. Data Collect.*, 2020, **30**, 100540.

20 J. I. Gowda, D. G. Gunjiganvi, N. B. Sunagar, M. N. Bhat and S. T. Nandibewoor, *RSC Adv.*, 2015, **5**, 49045–49053.

21 E. Nagles, M. Ceroni, J. J. Hurtado-Murillo and J. J. Hurtado, *Anal. Methods*, 2020, **12**, 2608–2613.

22 C. Zhu, G. Yang, H. Li, D. Du and Y. Lin, *Anal. Chem.*, 2015, **87**, 230–249.

23 H. Karimi-Maleh, F. Karimi, M. Alizadeh and A. L. Sanati, *Chem. Rec.*, 2020, **20**, 682–692.

24 N. Wongkaew, M. Simsek, C. Griesche and A. J. Baeumner, *Chem. Rev.*, 2018, **119**, 120–194.

25 N. T. Anh, N. X. Dinh, N. N. Huyen, P. T. L. Huong, V. N. Phan, P. D. Thang, H. Van Tuan, T. Van Tan, J. Lee and A.-T. Le, *J. Electrochem. Soc.*, 2023, **170**, 77506.

26 T. N. Pham, T. Q. Huy and A.-T. Le, *RSC Adv.*, 2020, **10**, 31622–31661.

27 J. M. Gonçalves, D. P. Rocha, M. N. T. Silva, P. R. Martins, E. Nossol, L. Angnes, C. S. Rout and R. A. A. Munoz, *J. Mater. Chem. C*, 2021, **9**, 7852–7887.

28 J. M. Gonçalves, L. V de Faria, A. B. Nascimento, R. L. Germscheidt, S. Patra, L. P. Hernández-Saravia, J. A. Bonacin, R. A. A. Munoz and L. Angnes, *Anal. Chim. Acta*, 2022, **1233**, 340362.

29 J. N. Baby, B. Sriram, S.-F. Wang and M. George, *Chem. Eng. J.*, 2022, **435**, 134136.

30 T. N. Pham, N. Van Cuong, N. X. Dinh, H. Van Tuan, V. N. Phan, N. T. Lan, M. H. Nam, T. D. Thanh, V. D. Lam and N. Van Quy, *J. Electrochem. Soc.*, 2021, **168**, 26506.

31 N. N. Huyen, N. T. Anh, T. L. H. Phung, N. X. Dinh, N. T. Vinh, T. T. Loan, D. L. Vu and A.-T. Le, *J. Electrochem. Soc.*, 2022, **169**, 106517.

32 N. T. Anh, N. N. Huyen, N. X. Dinh, N. T. Vinh, N. Van Quy, V. D. Lam and A.-T. Le, *New J. Chem.*, 2022, **46**, 7090–7102.

33 N. N. Huyen, L. M. Tung, T. A. Nguyen, T. L. Huong Phung, P. D. Thang, N. T. Vinh, Q. Van Nguyen, T. K. Oanh Vu, V. D. Lam, V. K. Le, N. X. Dinh and A.-T. Le, *J. Phys. Chem. C*, 2023, **127**, 12262–12275.

34 T. N. Pham, N. Q. Hoa, T. L. Nguyen, P. D. Thang, P. T. N. Trinh, D. T. N. Thanh and A.-T. Le, *RSC Adv.*, 2023, **13**, 10577–10591.

35 A. J. Bard, L. R. Faulkner and H. S. White, *Electrochemical methods: fundamentals and applications*, John Wiley & Sons, 2022.

36 E. J. J. Laviron, *J. Electroanal. Chem. Interfacial Electrochem.*, 1979, **101**, 19–28.

37 J. I. Gowda, R. M. Hanabaratti and S. S. Hipparagi, *Results Chem.*, 2023, **5**, 100801.

38 R. Wang, C. V. Reddy, A. Nagar, S. Basu, N. P. Shetti, B. Cheolho, J. Shim and R. R. Kakarla, *Chemosphere*, 2023, **341**, 139955.

39 V. Augustyn, P. Simon and B. Dunn, *Energy Environ. Sci.*, 2014, **7**, 1597–1614.

40 A. Sarkar and G. G. Khan, *Mater. Today Proc.*, 2018, **5**, 10177–10184.

41 E. Laviron, *J. Electroanal. Chem. Interfacial Electrochem.*, 1974, **52**, 355–393.

42 A. J. Bard, L. R. Faulkner and H. S. White, *Electrochemical methods: fundamentals and applications*, John Wiley & Sons, 2022.

43 M. Li and L. Jing, *Electrochim. Acta*, 2007, **52**, 3250–3257.